Q. J. R. Meteorol. Soc. (2000), **126**, pp. 2851–2872

Some impact of pollutants on the development and optical properties of stratocumulus clouds

By S. GHOSH[1]*, P. R. JONAS[1] and R. WOOD[2]
[1]*UMIST, UK*
[2]*Meteorological Research Flight, UK*

(Received 29 March 1999; revised 9 March 2000)

SUMMARY

Two major recent field programmes—the European Cloud Radiation Experiment (EUCREX) and the Aerosol Characterization Experiment II (ACE-2)—have extensively analysed the dynamical, microphysical and radiative attributes of stratocumulus clouds contaminated by continental air. Although an extensive set of dynamical and microphysical data are now available, there are no accounts of any matching theoretical modelling studies. To fully understand and numerically model the interplay between the dynamics, microphysics, radiative and chemical properties of the two clouds chosen for our case-studies would require a full three-dimensional large-eddy simulation (LES) model coupled to a full-size resolving microphysical model where the computational costs would be prohibitive. In this study we have 'optimized' the classic Kessler parametrization scheme so that it is effectively able to distinguish between clean and contaminated clouds. We perform LES runs with the optimized scheme to study the morphology and the dynamics of the clouds and then use a second one-dimensional microphysical parcel model run with identical environmental conditions to study the effects of pollution on the clouds as well as the droplet spectral evolution. This procedure yields extremely good agreement with observations at modest computational expense. It is shown that nitric acid (HNO_3) vapour in the parts per billion by volume (p.p.b.v.) range affects cloud formation by increasing the number of cloud droplets and decreasing the mean size compared to an acid-free simulation. The effects of HNO_3 contamination on the EUCREX case-study is evident owing to the proximity of this cloud to sources of air pollutants. With 10 p.p.b.v. of HNO_3, we are able to achieve good agreement with the observations of the droplet effective radii as well as with observations of the optical-depth variation. For the ACE-2 cloud which formed further away from sources of pollutants, even on a typical 'polluted' day when the ambient HNO_3 was ~5 parts per trillion by volume, the drop concentration was found to be insensitive to changes in the HNO_3.

KEYWORDS: Large-eddy simulation Kessler scheme Microphysics

1. INTRODUCTION

The importance of clouds in climate and weather processes has been recognized through a large number of observational and modelling studies. The radiation budgets at the top of the atmosphere are closely related to the cloud field. Clouds are also important physical elements in numerical weather prediction. Stratocumulus clouds have been the focus of attention because they significantly control the radiation budget of the earth and hence affect climate. As a result, over the past decade, along with numerous modelling studies (e.g. Moeng 1986), there have been many attempts to study these clouds experimentally (e.g. First ISCCP† Regional Experiment (FIRE I) (Albrecht *et al.* 1988); Atlantic Stratocumulus Transition Experiment (ASTEX) (Albrecht *et al.* 1995)). The radiative properties of a cloud field depend not only on the average microphysical properties of individual clouds but also on the spatial distribution of the clouds and the distribution of water within clouds (Cahalan *et al.* 1994). Water clouds, in particular semi-permanent stratocumulus sheets, dominate the global radiative-transfer process in solar wavelengths. Although such clouds may appear relatively uniform, they contain much variability in both water content and drop-size distribution (Davis *et al.* 1996; Marshak *et al.* 1997; Nicholls 1987; Brenguier *et al.* 2000). The details of the microphysical properties of clouds affect the cloud solar albedo (Twomey 1977) as well as the development of precipitation (Albrecht 1989). It is generally accepted that the droplet concentration in clouds that are formed in or pass over sources of

* Corresponding author: Department of Physics, UMIST, Manchester M60 1QD, UK.
† International Satellite Cloud Climatology Project.

pollutants is larger than that in clouds formed in clean air, and that these clouds have a correspondingly smaller droplet size for any given value of the liquid-water content. Reduction in cloud droplet size can be achieved when the air passes over sources of condensable vapours like nitric acid (HNO_3) as well as over sources of cloud condensation nuclei (CCN). Because of the rapid decrease in droplet encounter rates and collection efficiencies as the droplet size is reduced, formation of drops of precipitation size is inhibited in polluted clouds (Raga and Jonas 1993).

Although clouds are important elements in numerical weather prediction, not all aspects of cloud development and evolution are as yet completely understood. Climate is critically dependent on the properties of clouds. A small change in cloud parameters may significantly affect climatic temperature perturbations. For example, Slingo (1990) has shown that the effect of a 1–2 μm change in the effective radius of droplets in clouds may be comparable with that of doubling the CO_2 concentration.

In this study we have modelled the microphysical and radiative properties of two extensive stratocumulus clouds that have been studied experimentally by many research groups during the European Cloud Radiation Experiment (EUCREX) and the Aerosol Characterization Experiment II (ACE-2) campaigns respectively. The observations have been compared with our calculations using two separate numerical models. The first is a Large-Eddy Simulation (LES) model which is used to model in three dimensions (3-D) realistic representations of the cloud structure, showing very clearly convective cellular organization. The LES model also gives the appropriate dynamical parameters that are used as inputs to a parcel model of condensational growth having identical environmental conditions as in the 3-D LES run. We then have also considered the effect of HNO_3 on the droplet evolution, since observations of the synoptic conditions indicate the possibility of contamination of the EUCREX stratocumulus cloud and to some extent, on certain days, even the marine ACE-2 cloud. Our model runs clearly demonstrate, at least for the more polluted EUCREX cloud, that the effect of HNO_3 pollution on the droplet spectrum modification is significant, leading to the alteration of the microphysical and optical properties. In this paper we have tried to account for all these aspects and we do this in several stages.

The scheme of the paper is the following: first we discuss the applicability of using the classic Kessler scheme to model stratocumulus clouds using LES models. This is followed by a brief description of the 3-D LES model and the 1-D microphysical model. Next we use both the models applied to two case-studies.

The first case-study relates to the EUCREX cloud. Also, this being the more polluted of the two clouds, we discuss the implications of the effect of HNO_3 pollution on this cloud. We then compare model results with observations.

Then we move on to the more recent case-study of the ACE-2 cloud. We directly use the optimized LES model and present a detailed analysis of the structure, dynamics, microphysical and optical properties of the cloud. This is followed by a detailed comparison of the model results with the observations from the C-130 aircraft.

2. On the applicability of the classic Kessler scheme in LES of stratocumulus clouds

Many LES models which include warm-rain microphysics use the parametrizations proposed by Kessler (1969) which comprise a few simple algebraic equations to represent droplet growth through the autoconversion process, and raindrop growth through the accretion process. Although the scheme is simple and computationally inexpensive to use, one of its main limitations is that it is not able to distinguish between cloud

types. Secondly, the scheme is known not to perform too well for clouds with low liquid-water contents. Indeed, the original Kessler scheme was not even designed with stratiform clouds in mind and the autoconversion threshold in the original scheme was fixed at 0.5 g m^{-3} which is comparable to the average liquid-water contents of many stratocumulus clouds. In view of these limitations Feingold *et al.* (1998), based on an earlier work by Clark (1976), tried to bridge the gap between using simple Kessler-type schemes and the prohibitively expensive size-resolving microphysical schemes by proposing a new scheme which uses basis functions (log–normal or gamma) to describe the cloud and raindrop spectra. The details can be found from Feingold *et al.* (1998). *Although, this is an attractive alternative, it is still far more expensive than the simple* Kessler-type schemes and we feel that the procedure suggested by Feingold *et al.* (1998) is worth incorporating for a drizzling stratocumulus cloud—a situation when both cloud and rain or drizzle drops are present. And, as noted earlier, observations tend to indicate that drizzle is actually suppressed in stratocumulus clouds which have been contaminated with air pollutants. For a non-drizzling or a very weakly drizzling stratocumulus cloud we feel that use can still be made of the simple Kessler-type parametrizations after suitable modifications, and thereby make use of the considerable savings on computing resources to run the LES at higher resolution.

In this study we have 'optimized' the Kessler scheme by using the Berry (1968) scheme where the parametrization is based on mass, number and the relative dispersion of the droplets (which is a ratio of the standard deviation of the droplets and the mean radius) and not just on the water mass alone as in the original Kessler scheme, and accordingly it yields different results for clean and polluted clouds. In the original Kessler scheme there are two adjustable parameters—the autoconversion rate and the threshold, and both of them are often arbitrarily prescribed. In the optimized version the exact autoconversion rate is estimated for a given threshold. The details of this optimization procedure are described by Ghosh and Jonas (1998).

3. A BRIEF DESCRIPTION OF THE LES MODEL

The LES model that is used for this study is an adaptation of The Met. Office Large-Eddy Model (described by Mason(1989))with modified bulk cloud micro-physical and infrared (IR) radiation schemes. The details of the model are described in Pasquier (1996) and in Derbyshire *et al.*(1994) and will not be described here. The basic equations in this model are for a non-hydrostatic, anelastic atmosphere and the model equations are momentum conservation, mass continuity and the usual thermodynamic equations. In the subgrid model, the stresses and the subgrid scalar fluxes are estimated and the model is kept simple in order to devote computational resources to the explicit resolution of turbulence. The long-wave radiation parametrization scheme implemented within the cloud model is based on the method devised by Slingo and Wilderspin (1986). The lateral-boundary conditions in all the simulations in this study were periodic. The upper-boundary conditions are that the stresses and the heat flux are zero at the domain top. In addition, a process of damping was applied to a top layer of the domain so that instabilities did not extend beyond a selected height. The surface boundary conditions are those of the no-slip condition over a rough surface with roughness lengths estimated from observations for both momentum and temperature.

In this study, bulk-water rain microphysics was incorporated using the 'optimized' Kessler scheme described by Ghosh and Jonas (1998). This makes use of the observed droplet concentrations and the dispersion of the sizes (Table 1) to derive the autoconversion rate for a given autoconversion threshold for each case-study. In addition to the

TABLE 1. MODEL PARAMETERS OF THE DROPLET SPECTRUM AND THE CALCULATED PARAMETERS FOR THE OPTIMIZED KESSLER SCHEME FOR THE TWO CASE-STUDIES

Parameter	Value (EUCREX)	Value (ACE-2)	Value (Clean ACE-2)
Droplet concentration (cm^{-3})	200	120	50
Standard deviation of droplet radii (μm)	1.0	1.5	2.0
Autoconversion threshold ($g\ m^{-3}$)	0.33	0.33	0.33
Autoconversion rate (s^{-1})	5.46×10^{-4}	7.97×10^{-4}	1.1×10^{-3}

TABLE 2. INPUT PARAMETERS FOR THE LES 3-D SIMULATIONS

Parameter	Value (EUCREX)	Value (ACE-2)
Observational site	Guipavas, Brest	North of Tenerife
Sampling date	18 April 1994 (mission 206)	19 July 1997
Data from	Radiosonde	Cloudy-column flight C-130 aircraft
Vertical domain	3000 m	3000 m
Horizontal domain	10000 m	10000 m
Lateral domain	2500 m	2500 m
Δx	100 m	100 m
Δy	50 m	50 m
Δz	50 m (up to 1500 m) 107 m (above 1500 m)	50 m (up to 1500 m) 107 m (above 1500 m)
Time step	$\simeq$0.5 s	$\simeq$0.5 s
Temperature perturbation	$\pm$0.1 K at 52 m	$\pm$0.1 K at 52 m
Boundary condition at surface	Prescribed surface temperature obtained from sounding	Prescribed surface heat flux: latent-heat flux 76 W m^{-2} (from C-130 observations;) sensible-heat flux 2.2 W m^{-2} (from C-130 observations)
Depth of damping layer	500 m	500 m

autoconversion of the cloud drops to rain, the accretion of cloud droplets by rain and the evaporation of rain into dry air are also represented.

The model is initialized with observed vertical profiles of the total-water mixing ratio, the wind profile, and the dry potential-temperature profile. Convection was initiated with an initial temperature perturbation at a prescribed level just above the lower boundary. The input parameters for the two case-studies are shown in Table 2.

4. THE MICROPHYSICAL MODEL

The microphysical model used in this study considers a rising thermal as an expanding spherical mass, mixing with its surroundings as a result of turbulent motions generated within the thermal resulting in the exchange of heat, momentum and moisture. A critical assumption in this model is that the process of mixing with cloud-free air transfers droplets from the cloud to the drier environment where they evaporate and are replaced by fresh condensation nuclei of the same nuclear mass. In addition an entrainment process is also included with a rate given by $0.6\,U/R$ where U and R are the updraught speed and the initial thermal radius, respectively. Further details of this

model can be found in Mason and Jonas (1974) who developed the original version of this model. The thermal initial radius for the two clouds was derived from the layer-averaged values of the dissipation energy, ϵ, and the standard deviation of the in-cloud vertical velocity, σ_w, obtained from the LES model.

Observations of the synoptic conditions for these case-studies indicates the possibility of contamination by polluted air from the continent. This is certainly more evident for the EUCREX cloud. In the next section we give an account of the changes initiated in the microphysical model results when we consider the effect of HNO_3 vapour on the CCN activation. In the microphysical model runs, the same initial environment was prescribed for the runs with and without the acid since the presence of HNO_3 at the low levels considered is not likely to affect the initial dynamical inputs.

(*a*) *Implications of including HNO_3 in the microphysical model*

It is now well known that oxides of nitrogen (NO_x) are the most important sources of HNO_3 and that the increase of NO_x alters the ambient HNO_3 concentrations. Penner *et al.* (1991) have shown that during the month of July the concentration of HNO_3 over continents exceeds 1.0 parts per billion by volume (p.p.b.v.). On the other hand, in heavily polluted areas the concentration can even be as high as 50 p.p.b.v. (Seinfeld 1986; Mackay *et al.* 1988). From an analysis of the synoptic conditions over the region of interest for the EUCREX cloud, we find a strong north-east flow indicating that by the time the cloud has fully formed over the measuring station at Guipavas, Brest, it is very likely that the incoming air would be contaminated by air pollutants (including HNO_3) from the continental air. Unfortunately, the HNO_3 concentration was not measured within the stratocumulus cloud during the EUCREX campaign. However, as a conservative estimate, it is very likely to be within the range 1–10 p.p.b.v. In this study we therefore investigate the effects of introducing 10 p.p.b.v. HNO_3. For the more recent ACE-2 campaign, observations suggest that the contamination is less severe since this cloud was much further from pollution sources. As a result the observed levels of HNO_3 concentration are of the order of 5 parts per trillion by volume (p.p.t.v.) (Dore *et al.* 1998).

The process of CCN activation is initiated in the model by invoking the Kohler theory. The theory suggests that, as the saturation ratio S of water increases, the CCN particles being hygroscopic absorb water and are close to equilibrium with the environment; when S exceeds a critical value for a given nuclear mass the particles start to grow spontaneously, stopping only when the water vapour has been sufficiently depleted. The critical values of the radius and the supersaturation ratio are $r^* = (3b/a)^{1/2}$ and $S^* = 1 + (4a^3/27b)^{1/2}$ where a and b are constants depending on the mass and composition of the nucleus. Kulmala *et al.* (1993) invoked the standard Kohler theory but included the effect of HNO_3 as a second condensing vapour. When acid vapour is present in the system and condenses simultaneously with water, all the thermodynamic variables now refer to the ternary solution enabling one to draw Kohler curves at fixed prescribed values of the acid concentration. In essence the presence of the acid vapour modifies the reduction in the saturation vapour pressure due to the dissolved material. We estimate an effective value of the solution parameter, b, as a weighted mean from known masses of the salt and HNO_3 and then calculate a new value of the critical supersaturation. The procedure is repeated for each of the 60 size classes of the salt and for prescribed values of HNO_3 concentrations. Our approach is broadly similar to that of Kulmala *et al.* (1993), except that while these authors considered a $NaNO_3$ aerosol spectrum, we have assumed a NaCl spectrum for the EUCREX case-study since

TABLE 3. INPUT PARAMETERS FOR THE MICROPHYSICAL MODEL

Parameter	Value (EUCREX)	Value (ACE-2)
Environmental temperature at cloud base	1.1 °C	13.5 °C
Environmental pressure at cloud base	920.3 mb	911.5 mb
Environmental lapse rate	5.8 degC km^{-1}	5.2 degC km^{-1}
Initial updraught speed (U)	0.6 m s^{-1}	0.95 m s^{-1}
Thermal initial radius (R)	311 m	305 m
Aerosol composition	NaCl	$(NH_4)_2SO_4$ + NaCl
HNO_3	10 p.p.b.v.	5 p.p.t.v.

we do not have any observations of the aerosol composition. However, for the ACE-2 project observations are available for the size distribution and chemical composition of the aerosol and we have used a mixed spectrum of $(NH_4)_2SO_4$ and NaCl. In addition, for both the case-studies we have considered the effects of entrainment in our model runs which was not considered by Kulmala *et al.* (1993).

The input parameters for the microphysical model are summarized in Table 3.

5. CASE-STUDY I: EUCREX

The EUCREX experiment was performed in April 1994 at Brest, France. On 18 April, an anticyclone was located on the west of Brittany maintaining a stationary north-easterly flow over the English Channel and Brittany, with extensive stratocumulus at the southern edge. Satellite observations show that the cloud thinned towards the north-west. Aircraft measurements were made between 0930 and 1200 UTC along a line extending approximately north-west from the airport at Guipavas. At the north-west limit of the flights the cloud became increasingly broken. The cloud base varied between 600 and 800 m and the top between 1000 and 1100 m. The maximum liquid-water content (LWC) varied between 0.5 and 0.6 g m^{-3} and no ice was observed anywhere within the cloud. The maximum droplet concentration was observed to be $\sim$500 cm^{-3} suggesting the influence of the passage of the air over sources of pollution. Further details of the observed features of the cloud can be obtained from the study by Pawlowska and Brenguier (1996).

In Fig. 1 we show the 3-D cloud liquid-water field after four hours of simulation using the optimized Kessler scheme and model parameters from Table 2. The simulation shows a solid cloud layer with an undulating cloud top. The boundary-layer eddies, and in particular the larger ones, are driven in part by the destabilization of the cloud layer and by cloud-top radiative cooling. The undulations of the cloud top occur only when the boundary-layer eddies are fully developed. The 3-D simulations show very clearly these cloud-top undulations which match qualitatively with the observations. The computed values of the cloud liquid-water content ($\sim$0.25–0.30 g m^{-3}) and the cloud depth ($\sim$300 m) agree well with the observations presented by Pawlowska and Brenguier (1996).

(*a*) *Microphysical-model results*

From the procedure outlined in section 4 and the input parameters listed in Table 3 we were able to quantify the effect of HNO_3 on CCN activation and the subsequent drop-size distribution. First, we show in Table 4 the number of activated CCN as a function of acid concentration and height above the cloud base.

From Table 4 we find that even with modest amounts of HNO_3 in the simulation the total number of activated CCN increases. We now turn to the issue of the changes

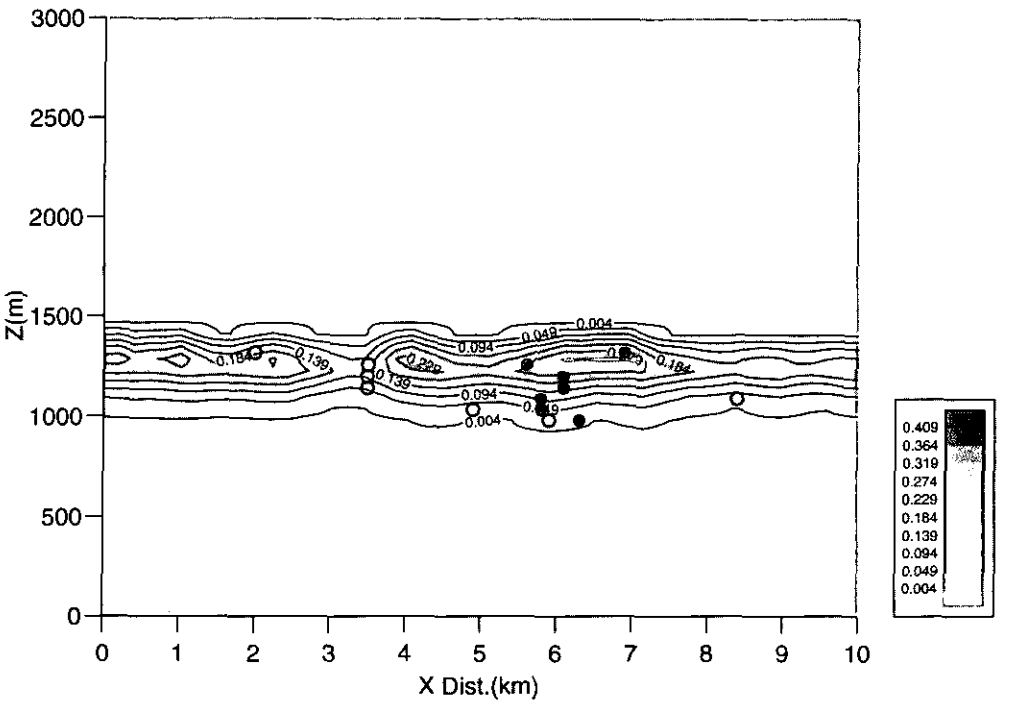

Figure 1. Liquid-water content (g m^{-3}) from the LES model after four hours for the EUCREX cloud (see text for explanation). Open (solid) circles indicate regions of minimum (maximum) liquid-water content.

TABLE 4. NUMBER OF ACTIVATED CLOUD CONDENSATION NUCLEII AS A FUNCTION OF ACID CONCENTRATION AND HEIGHT ABOVE THE CLOUD BASE (h)

HNO_3 Concentration (p.p.b.v.)	Number activated (cm^{-3})		
	$h = 50$ m	$h = 100$ m	$h = 200$ m
0	392	475	409
10	528	514	520

in the droplet spectrum initiated by the acid vapour. In Fig. 2 we show the calculated droplet spectra at 100 and 200 m above the cloud base. We find that at 100 m above the cloud base the peak in the concentration distribution is at about 4.0 μm radius with the highest number density ~120 cm^{-3} for the run with 10 p.p.b.v. of HNO_3. When no acid is included the peak is observed at larger sizes at around 5.0 μm radius with a smaller number density ~90 cm^{-3}. A similar feature is also observed at 200 m above the cloud base, and by comparing the spectra at these two levels we find that there are more of the larger drops towards the cloud top—a feature which is generally observed for stratocumulus clouds. The peak number density ~125 cm^{-3} at 4.0 μm radius is achieved only when 10 p.p.b.v. of HNO_3 is introduced in the simulation. The range of predicted droplet sizes with radii between 4 and 7 μm is in broad agreement with the observations from Pawlowska and Brenguier (1996), although the maximum observed number concentrations were sometimes higher. Possibly there were other pollutants in addition to HNO_3 which we have not considered and further, without any observations

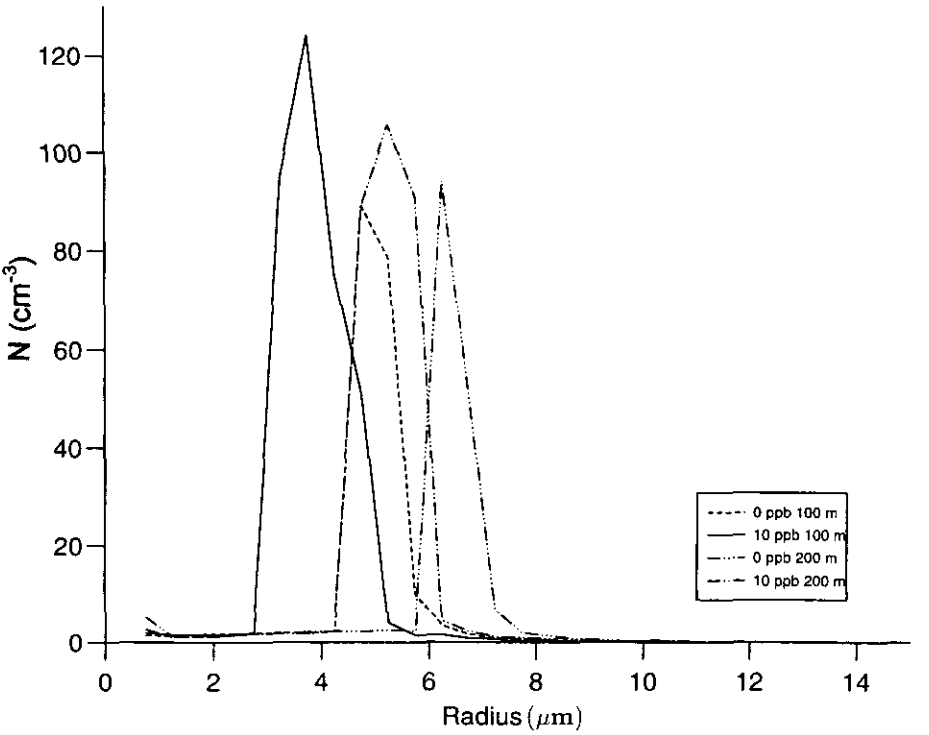

Figure 2. Modelled droplet spectra for the EUCREX cloud (see text) at 100 and 200 m above the cloud base, with acid at 10 p.p.b.v. and without.

on the chemical composition of the CCN spectrum, we initialized our model with an assumed pure NaCl spectrum. However, our model runs show that even with a modest 10 p.p.b.v. of HNO_3, the droplet number concentrations increase by about 35% with an associated reduction of droplet radii by about 1.0 μm.

The microphysical-model results are consistent with the fact that the presence of HNO_3 vapour would tend to decrease the effective vapour pressure of water over the growing solution droplets. As a consequence of this, a higher fraction of NaCl particles can serve as CCN than in an acid-free environment. Our calculations show that the overall effect of HNO_3 is to decrease the mean size of droplets, as the available vapour is now distributed between a larger number of activated NaCl particles. The overall effect of air pollutants to increase droplet number concentrations is well borne out by our model simulations, and is also observed in the experimental studies of Leaitch *et al.* (1992).

The fact that enhanced levels of HNO_3 would increase the number concentration and decrease the droplet mean size may have far-reaching implications for the radiative properties of low clouds. These effects can inhibit precipitation because smaller droplet sizes lead to a longer cloud life. This is in addition to the direct impact on the solar albedo of increasing droplet concentration while maintaining the LWC. These discussions lead us to examine some critical parameters that control cloud radiative properties. We present calculations with and without the presence of HNO_3 and then compare our model results with the experimental data from aircraft.

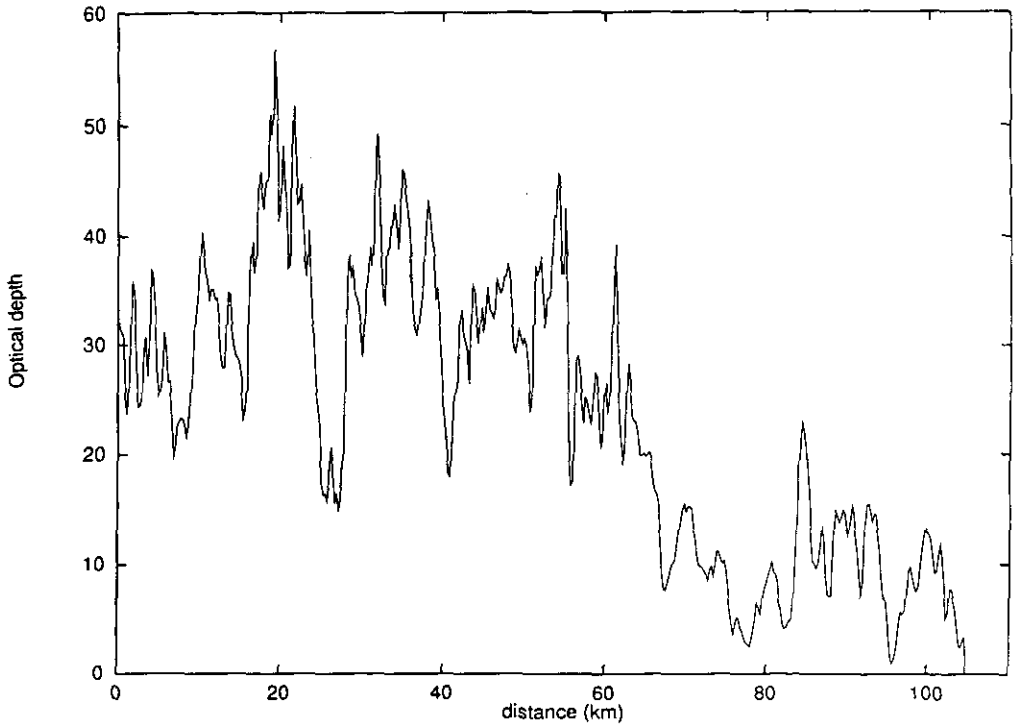

Figure 3. Observed optical depths for the EUCREX cloud from the POLDER instrument on board the ARAT aircraft. See text for further explanation.

We shall summarize two sets of results—the first pertaining to remote sensing from above the cloud obtained from the ARAT (Fokker 27) instrumented aircraft, and the second to the *in situ* measurements from the Meteo-France Merlin-IV with the Fast Forward Scattering Spectrometer Probe (FSSP). We shall then compare our model calculations with both these sets of observations.

(*b*) *Remote-sensing measurements and the estimation of the cloud optical depth*

The most general way of estimating the cloud optical depth τ is given by

$$\tau = \frac{3}{2} \int \frac{q_\ell(z)}{\rho_w r_e(z)} \, dz, \tag{1}$$

where ρ_w and q_ℓ are the liquid-water density and the LWC, respectively, r_e is the droplet effective radius, and the integration extends from the cloud base to the cloud top. This equation for solar visible wavelengths is strictly valid for a non-absorbing medium where the drop size is much bigger than the wavelength. The radius r_e is the ratio of the third to the second moment of the size spectrum and is related to the mean-volume radius r_{vol} (and hence q_ℓ) by

$$\frac{r_{vol}^3}{r_e^3} = k, \tag{2}$$

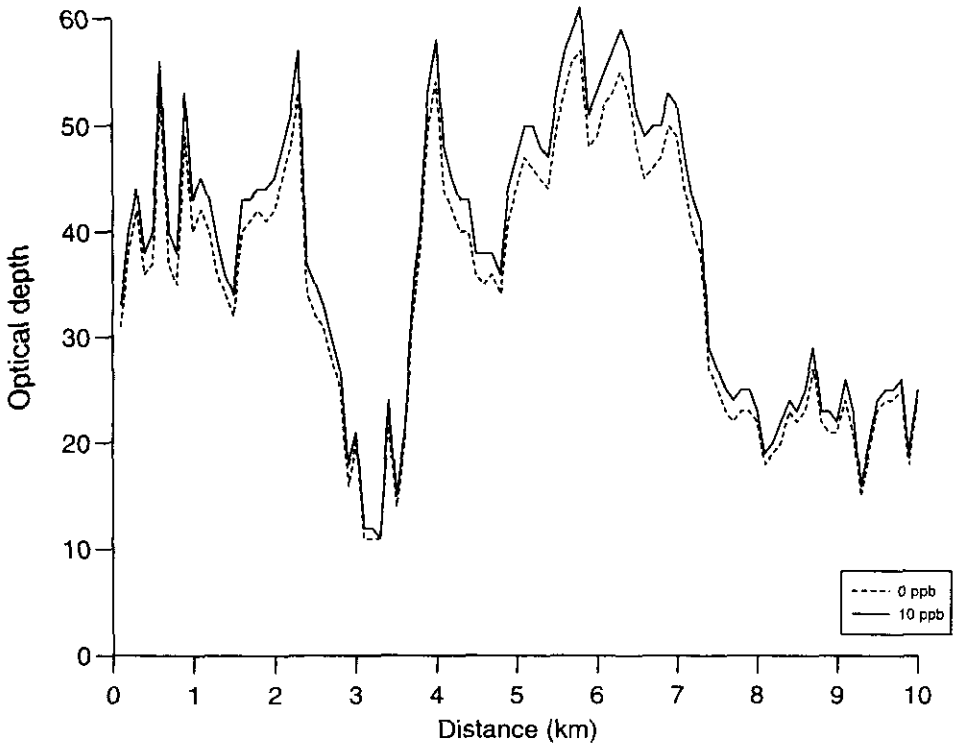

Figure 4. Modelled optical depths for the EUCREX cloud (see text), with acid at 10 p.p.b.v. and without.

where $k \sim 0.9$ for continental clouds and the mean-volume radius is given by

$$r_{\mathrm{vol}} = \left(\frac{3q_\ell}{4\pi N \rho_{\mathrm{w}}} \right)^{1/3}, \tag{3}$$

where N is the droplet number concentration. While q_ℓ and the cloud geometric thickness across the cloud are obtained from the LES outputs, values of N, which depend on the HNO_3 concentration, are estimated from the microphysical model, and the optical depth is then calculated from Eqs. (1)–(3).

From the definition of the optical depth it is clear that it depends sensitively on the distribution of cloud liquid water as well as on the cloud geometric thickness, and the success of model estimations will depend on how accurately the model estimates these quantities.

First we describe observations from the Polarization and Directionality of the Earth's Reflectance (POLDER) instrument on the ARAT aircraft; details of the instrument can be obtained from Deschamps *et al.* (1994) and Descloitres *et al.* (1996). It must be borne in mind that the observational data span a horizontal extent of about 100 km across the mean wind direction whereas the horizontal extent of the LES model run is only 10 km. However, since the 3-D LES runs were subject to periodic boundary conditions, the simulated cloud structure would repeat itself in 10 km intervals. In view of this it seems reasonable to study the modelled optical-depth variability spanning 10 km with the observed values. We must also point out that although each cloud target was observed using 17 different viewing angles we report observations from the middle viewing angle only.

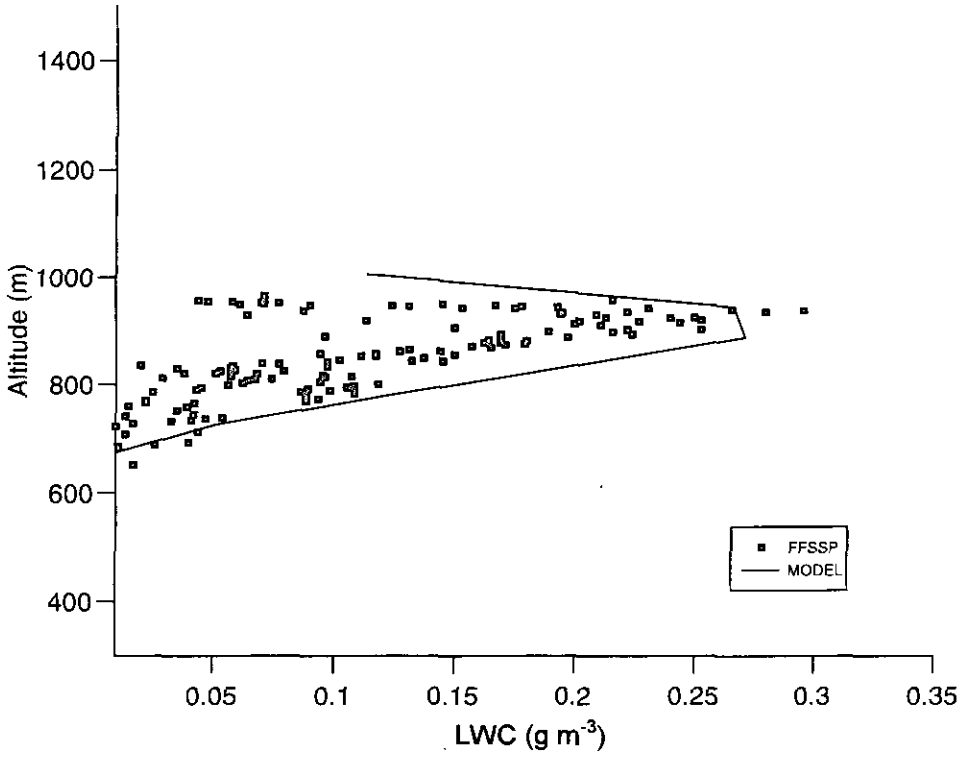

Figure 5. Liquid-water content for the EUCREX cloud from the LES model compared with *in situ* Fast FSSP measurements. See text for explanation.

Figure 3 shows the observed cloud optical depths across 100 km. However, in order to achieve a meaningful comparison between the observations and the model, we avoid regions with large extremes of optical depth, observed especially near the start and the end of the flight, and confine ourselves to between 20 and 65 km. Several interesting features emerge from Fig. 3. First, we observe a significant variation in the optical depths with the lowest values ~10 and the highest ~58. This is also generally true for the model results shown in Fig. 4. Although the variations are more pronounced in the model owing to its higher resolution of 100 m compared with a horizontal resolution of about twice this size in the POLDER observations, the model is able to capture the overall range of the optical-depth variations. In general it is found that the acid-free simulations have about 7% smaller optical depths than those which contained HNO_3, and optical depths approaching 60 could be attained in the model results only after 10 p.p.b.v. of HNO_3 was introduced in the microphysical simulation.

(*c*) In situ *measurements*

So far we have discussed remote-sensing measurements of the cloud optical depth. We now turn to the *in situ* measurements to examine other important parameters, like the droplet effective radius and the liquid-water content.

These measurements have been made on board the Merlin-IV with the Fast FSSP that provides much better accuracy than the standard probe. Although vertical sampling was not possible with the aircraft, rapid ascents and descents provide satisfactory sampling of the vertical evolution of the droplet spectra (Pawlowska and Brenguier

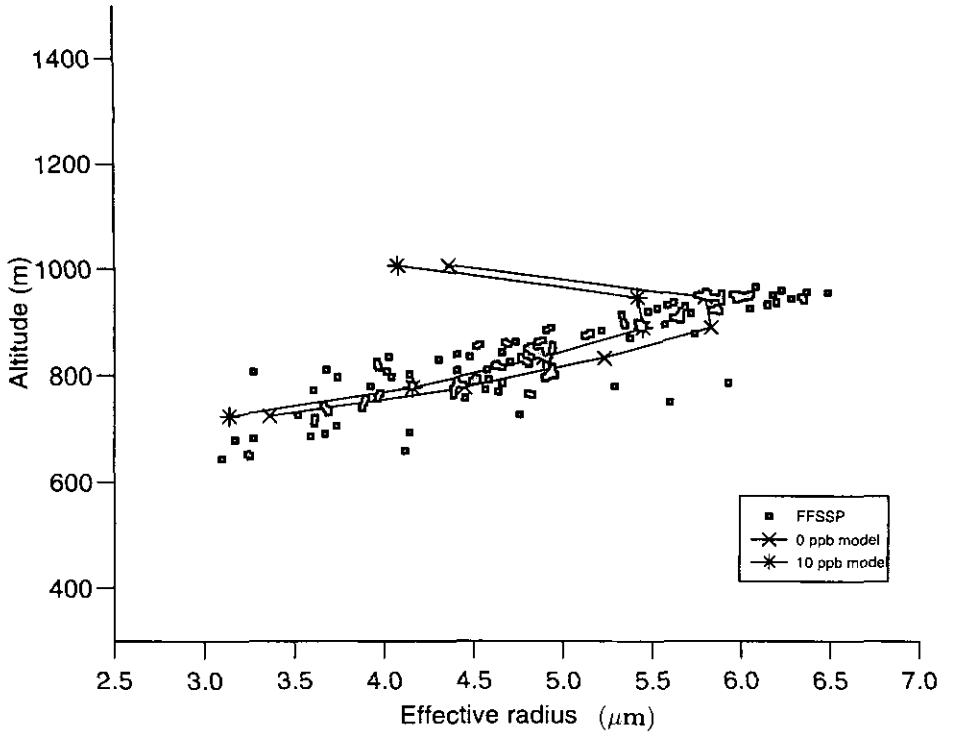

Figure 6. Comparison of modelled and observed droplet effective radii for the EUCREX cloud, with and without acid (see text).

1996). In this paper we are primarily concerned with the in-cloud properties (spanning a vertical extent of ~350 m between the cloud base and the cloud top) and therefore we chose a sampling domain confined within the last leg of the flight which follows a zig-zag pattern of very short duration. We compared the model results with observations corresponding to the data sampled for the starting times 1140:06, 1141:57, and 1143:47 UTC. The sampling rate was 1 Hz (100 m horizontal resolution).

Figure 5 shows the LWC from the Fast FSSP measurements as well as the layer-averaged LWC from the LES. We find good agreement between the modelled and observed values although the cloud is slightly deeper in the model. When we refer back to Fig. 1, where we have shown the instantaneous values of the LWC, we find that the lowest values of the LWC are generally found in regions where the effects of entrainment are the most pronounced (see the locations of the open circles in Fig. 1), and likewise the regions of the highest LWC which are ~0.3 g m^{-3} are located deep within the cloud where entrainment effects are minimal. This shows that the LES model correctly represents the effects of entrainment and as a result we find the overall good agreement between modelled and observed values of the cloud LWC shown in Fig. 5.

In Fig. 6 we show a comparison between the observed and modelled values of r_e. From Fig. 6 it is clear that the modelled r_e agree reasonably well with the observations, and the run which includes 10 p.p.b.v. of HNO_3 is able to yield the observed smallest values of r_e close to 3 μm which are not predicted by the acid-free run. Very close to the cloud top, observations show r_e in excess of 6 μm which the model is not able to capture. This is due to the vertical resolution of 50 m in the vertical for the model runs.

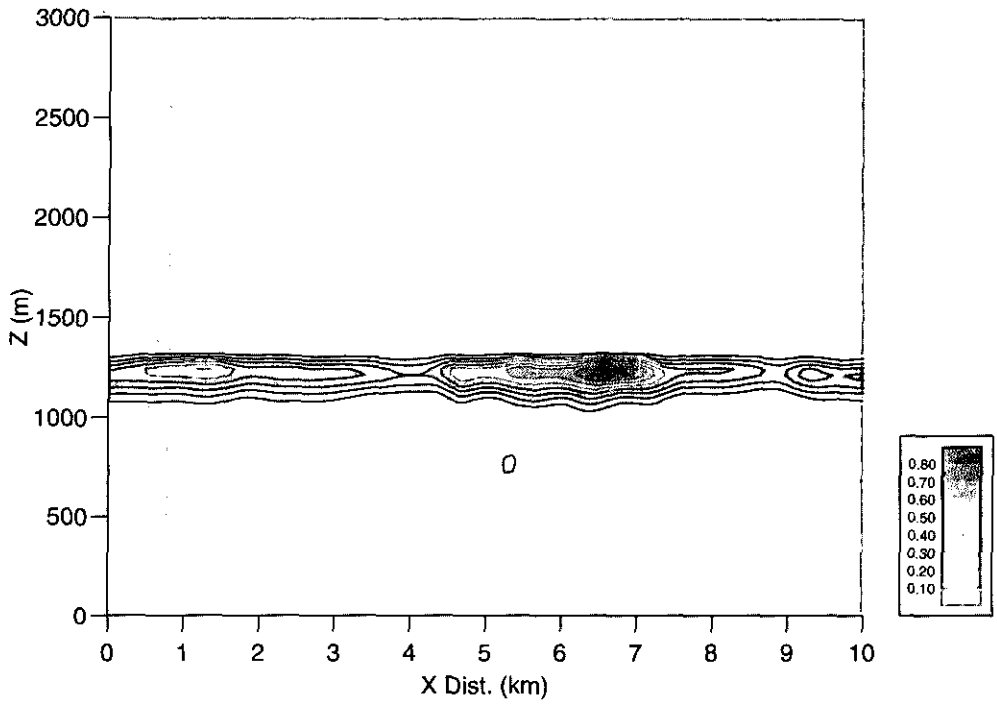

Figure 7. Liquid-water content (g m^{-3}) from the LES model after four hours for the ACE-2 cloud (see text).

A finer mesh possibly could have better captured the very sharp inversion close to the cloud top. For the same reason we notice some underprediction in the cloud-top LWC (Fig. 5).

6. CASE-STUDY II: ACE-2

The ACE-2 Field campaign was aimed at studying the direct and indirect effect of aerosols on climate and was conducted from the 15 June to 23 July 1997 in the north-east Atlantic region near the Canary Islands (see Raes *et al.* 2000). Although the air in the boundary layer originated from the Atlantic and the stratocumulus cloud was relatively 'clean', on some days observations indicate the possibility of advection of polluted continental air from Europe. The initial sounding used for the LES model was obtained from the C-130 aircraft observations on 19 July 1997 and corresponds to a contaminated case with an observed droplet concentration $\sim$120 cm^{-3}.

Figure 7 shows the cloud LWC calculated from the optimized 3-D model after four hours of simulation and we find that this is a thinner cloud than the preceding case, although the LWC is higher due to the higher cloud-base temperature. In Fig. 8 we show the LWC in the x–y plane at 1144 m, the mid-cloud level. This figure clearly demonstrates that the discretization is sufficient to yield resolved eddies of varying sizes throughout the cloud layer and also that the resolved eddies are nearly isotropic in the horizontal, although there is a suggestion of roll-like structures in the across-wind direction.

Observational data from the ACE-2 project are being processed by various research groups and many of the data are still unpublished. However, we have tried to compare

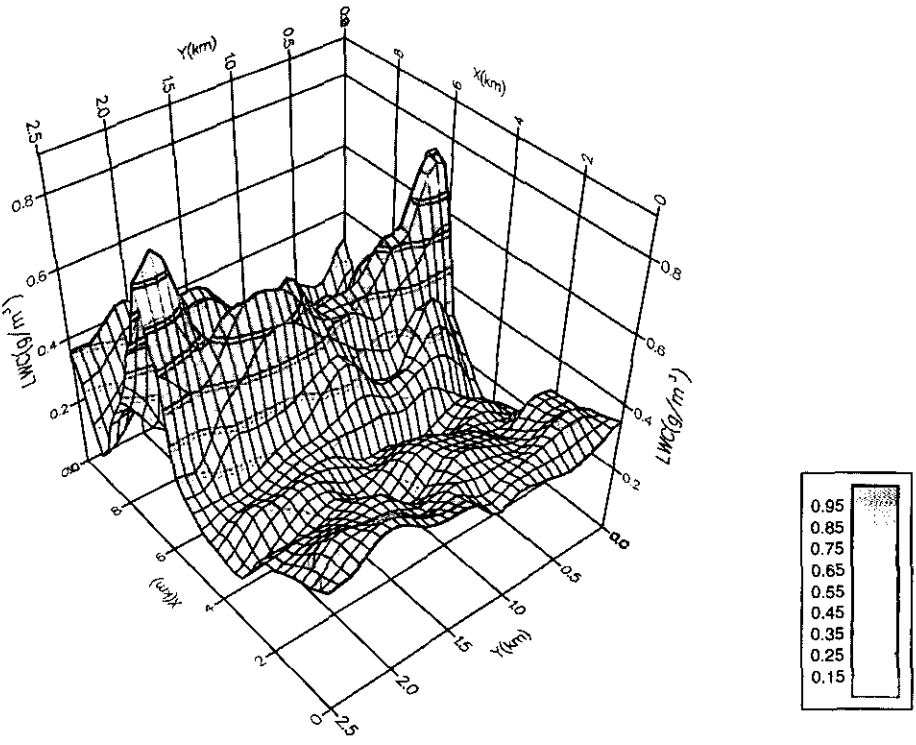

Figure 8. As Fig. 7, but in the x–y plane at 1144 m.

our model results with observations from the C-130 aircraft for 19 July. In Fig. 9 we have shown the layer-averaged LWC profile which agrees remarkably well with observations taken during a profile with the Johnson–Williams LWC instrument. The observed cloud base was at a height of approximately 950 m and the top at 1200 m. This is in very good agreement with the modelled values given the 50 m vertical resolution of the model. In fact, the optimized model is able to capture the moistening of the sub-cloud boundary layer which was observed, and results in non-zero values of the average LWC at some levels below the main cloud base. In Fig. 9 we have also plotted the adiabatic profile and we find that both the modelled and the observed profiles in the cloud layer are almost adiabatic. Pawlowska and Brenguier (1998) also independently report that the measured values of the LWC were often very close to adiabatic. Examination of the model vertical-velocity fields shows that the downdraughts are stronger than the updraughts but that the updraughts extend from the lower-boundary layer up to the cloud top. These updraughts are likely to carry moisture from the sea surface upwards, explaining the moistening of the subcloud layer shown in Fig. 9.

(*a*) *Optical-depth estimation from aircraft data and from the LES model*

Although the cloud optical depth can be estimated from Eq. (1), simplifications can be made for an adiabatic cloud. The following assumptions were made in order to estimate the cloud optical depth from the aircraft measurements: (i) cloud-top height (i.e. the inversion) is at a constant height determined from an aircraft profile through the cloud layer, but cloud base is variable; (ii) the height of the aircraft above cloud

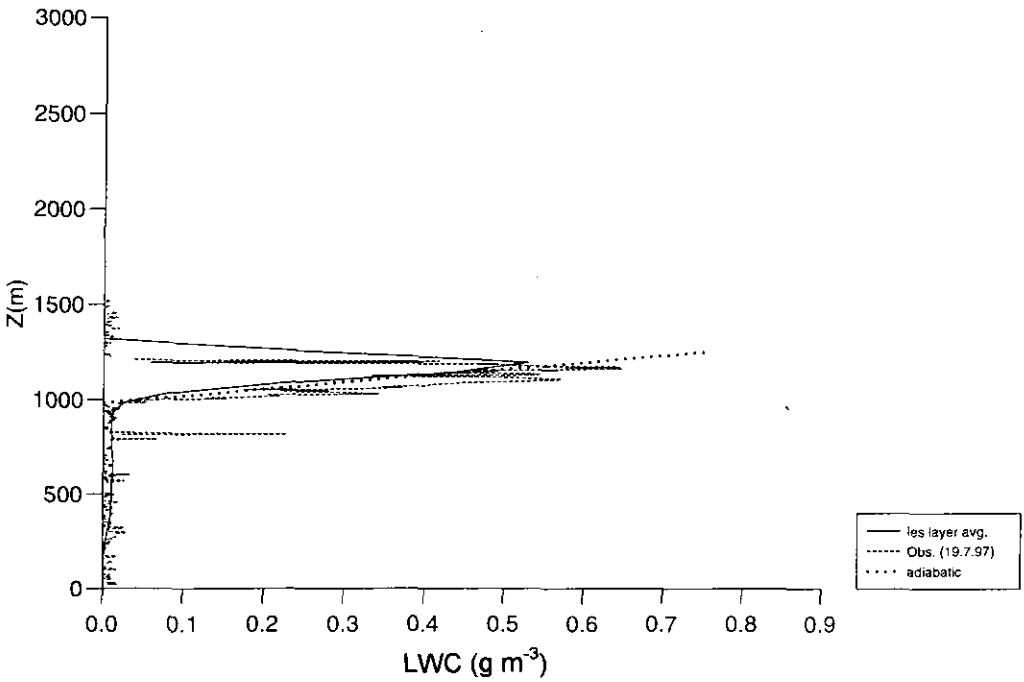

Figure 9. Layer-averaged liquid-water content (LWC) calculated from the LES model for the ACE-2 cloud compared with the observed Johnson–Williams LWC.

base, when in adiabatic regions of cloud, is determined purely from the LWC and the adiabatic rate of increase of the LWC with height (denoted by Γ_ℓ).

For an adiabatic cloud the LWC can be expressed as

$$q_\ell(z) = \Gamma_\ell(z - z_{\mathrm{cb}}), \tag{4}$$

where z is height and z_{cb} is cloud-base height. The value of Γ_ℓ is a function of temperature and pressure and is around 2.5×10^{-3} g m^{-3} for stratocumulus clouds. Stratocumulus clouds typically have thicknesses of around 500 m or less so the change in Γ_ℓ from cloud base to cloud top is generally small. The effective radius and the mean-volume radius (and hence the LWC) for maritime stratocumulus clouds are related to each other (see Eqs. (2) and (3)).

From the above considerations, with the assumption that Γ_ℓ is constant with height, and after some algebra, it is easy to show (e.g. Pawlowska *et al.* 2000; Brenguier *et al.* 2000) that the optical depth can be expressed as

$$\tau = \left(\frac{243\pi}{250}\right)^{1/3} \left(\frac{kN}{\rho_{\mathrm{w}}^2}\right)^{1/3} \Gamma_\ell^{2/3}(z - z_{\mathrm{cb}})^{5/3}, \tag{5}$$

where $k \sim 0.8$ for maritime stratocumulus clouds (Martin *et al.* 1994). Thus, the most important parameter in determining the optical thickness of a stratiform cloud is the thickness, since τ has a 5/3 power-law dependence upon this parameter.

Pawlowska *et al.* (2000) and Brenguier *et al.* (2000) found that subadiabatic regions with the stratocumulus clouds studied were characterized by a reduction in droplet concentration due to mixing and dilution with dry regions. From all the in-cloud aircraft data (profiles and straight and level runs) adiabatic regions were selected where the

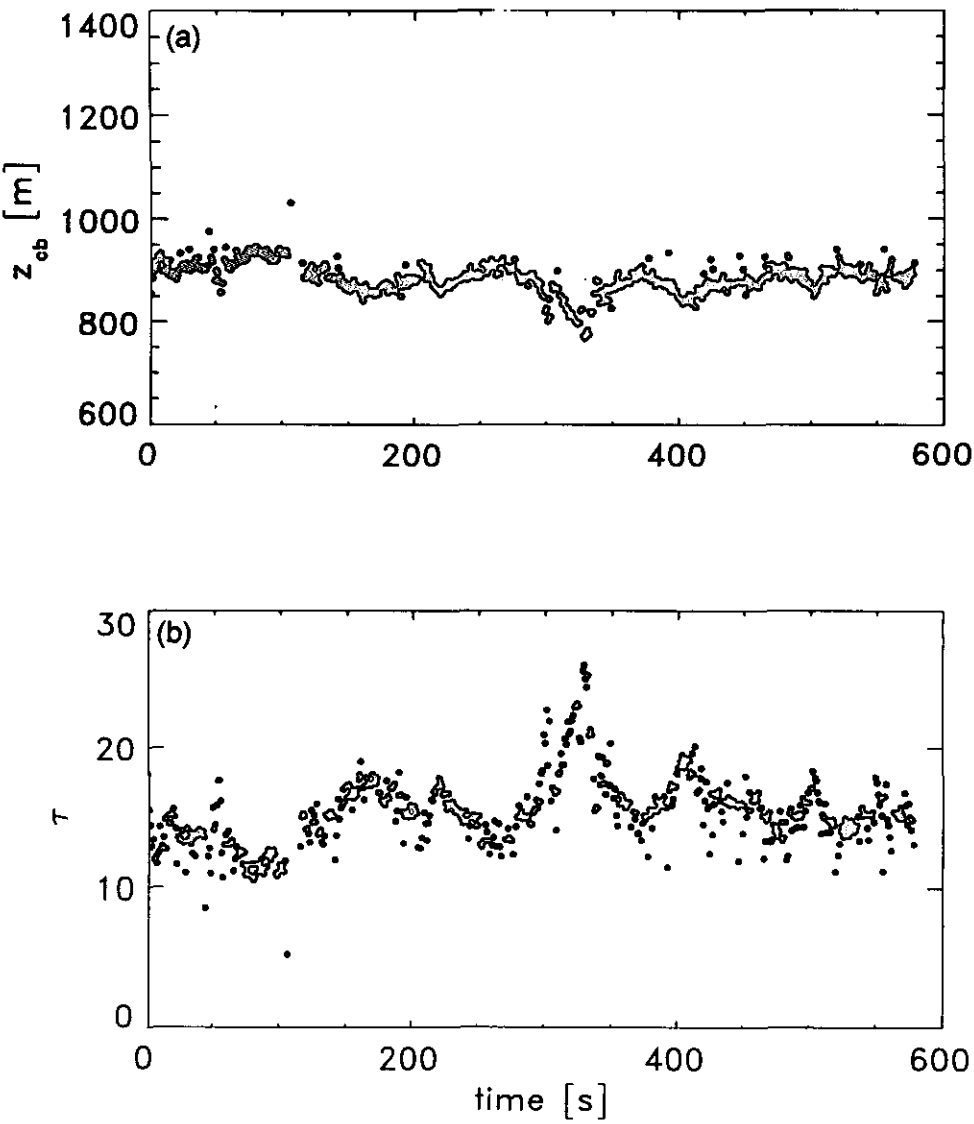

Figure 10. Examples of derived (a) cloud-base height and (b) optical depth from one of the in-cloud straight and level runs.

droplet concentration exceeded 60% of the maximum value. The cloud base for these regions was determined using Eq. (4). From the derived cloud base and assumption (i), the optical depth was estimated using Eq. (5). Figure 10 shows derived cloud-base height and optical depth from one of the in-cloud straight and level runs. A constant droplet concentration of 120 cm^{-3} was used in the calculation which was the observed mean for the adiabatic regions. In order to compare with the LES model results, the observational data were split into sections of 10 km length (~100 s) to remove large-scale fluctuations which cannot be captured with the small LES domain. The mean optical depth from the aircraft measurements was 12.6. From each 10 km section the standard deviation of optical depth was calculated and ranged from 0.8 to 8.0 with a mean of 2.6.

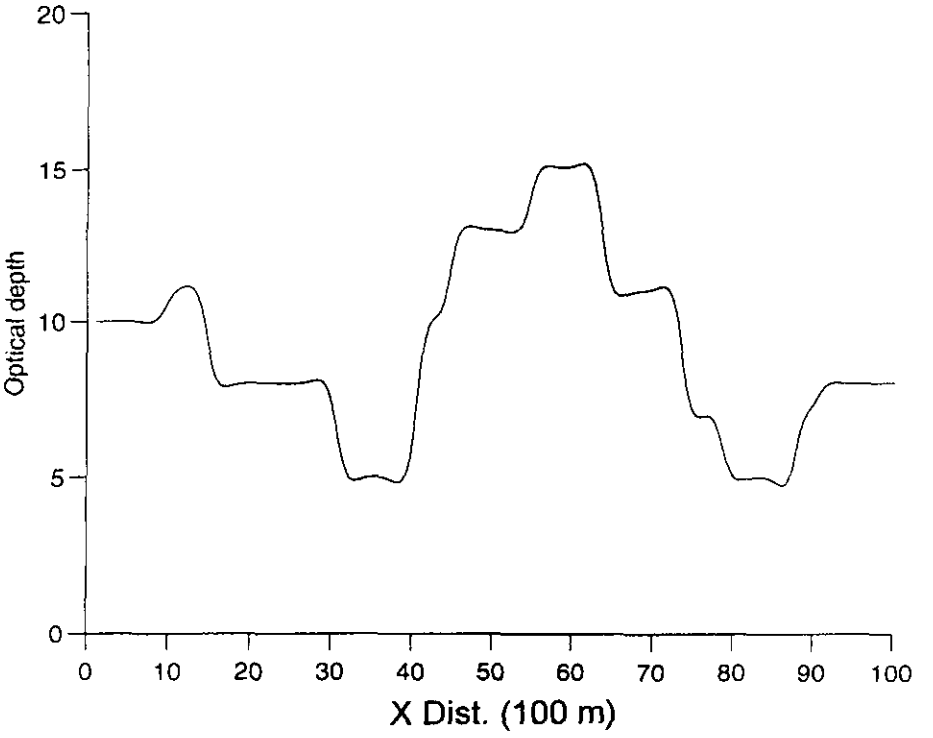

Figure 11. Horizontal variation of the modelled optical depths for the ACE-2 cloud. The mean is 9.18 and the standard deviation is 3.04.

Optical depths were also available from the OVID multi-spectral radiometer (Schüller *et al.* 1997, 2000) which flew above the cloud during C-130 measurements. The mean observed optical depth was 8.6. Again, 10 km sections were used to obtain a standard deviation. The range of standard deviations of the 10 km sections was 0.7–8.8 with a mean of 2.5. The OVID observations necessarily include subadiabatic regions, which is the most likely reason why the C-130 mean estimated optical depth is higher than the radiometric measurement.

Optical depths were calculated from the LES model. First, we present the simplified treatment invoking the adiabatic assumption using Eq. (5) where we assume the same number concentration as in the observations (i.e. 120 cm^{-3}) but we use the cloud thickness, Δz, from the LES model. This is shown in Fig. 11 where we show the variation of the modelled optical depth across a horizontal distance of 10 km. The mean and standard deviation of the modelled optical depth are 9.18 and 3.04, respectively, in reasonable agreement with the observations from OVID. While the C-130 measurements cannot be used as a direct validation of the LES model owing to the removal of subadiabatic regions, they do appear to show that the adiabatic assumption results in reasonable values of optical depth and of its spatial variability.

Using the modelled LWC and Eq. (1), a full map of optical depth was obtained covering a 10×2.5 km domain, without invoking the approximations relevant to an adiabatic calculation. This is shown in Fig. 12 and we immediately observe a great variability in the optical depths. The simplified layer-averaged adiabatic calculations, shown for the aircraft data as well as for the model, tend to obscure the geometric variability.

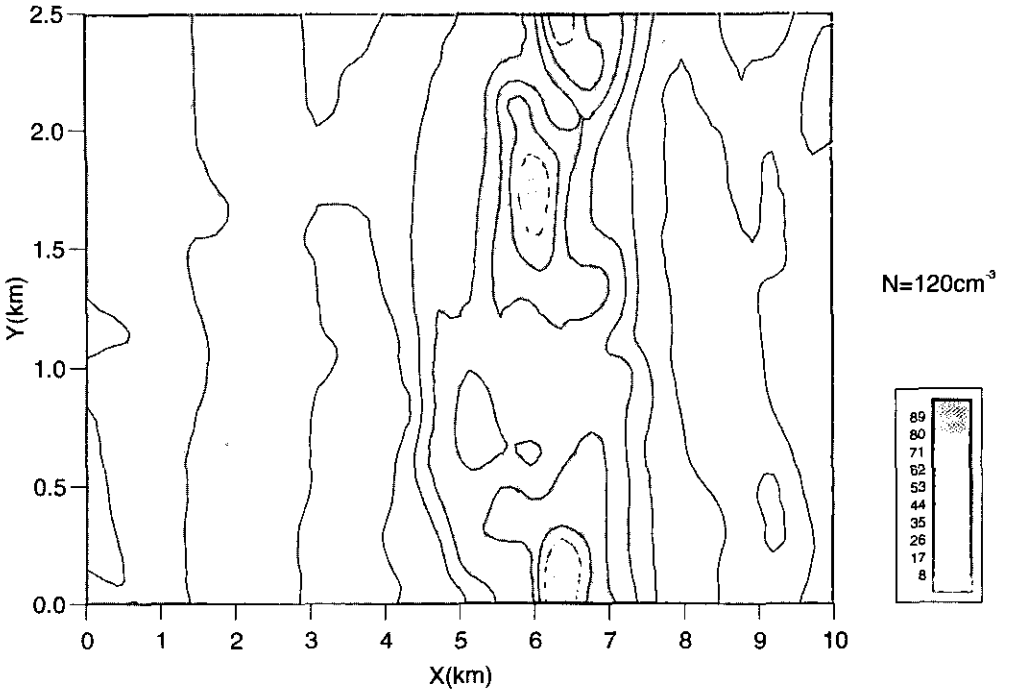

Figure 12. Optical depth map in the x–y plane for the ACE-2 cloud calculated from the LES model. See text for explanation.

The optical-depth variability depends largely on the variability of the geometric cloud thickness as well as the variability of the liquid-water distribution. The largest optical depths are located between 5 and 7 km in the x-direction. Unfortunately we do not have a map from the observations to compare with our model results. The modelled optical depths shown in Fig. 12 suggest that any future work on the ACE-2 cloud aimed at studying the optical properties of the cloud should take cognizance of this enormous variability.

(*b*) *Sensitivity of the ACE-2 cloud to pollutants*

One of the aims of this work has been to demonstrate the usefulness of the optimized microphysical scheme in the 3-D LES model which can differentiate between clean and contaminated clouds. The ACE-2 results presented so far refer to an optimization compatible with a contaminated maritime stratocumulus cloud for which the cloud-water autoconversion rate $\sim 7.97 \times 10^{-4}$ s^{-1}, where the average droplet size and the number concentration are 7 μm radius and 120 cm^{-3}, respectively. However, for a 'clean' cloud with larger ($\sim$9.4 μm radius) and fewer ($\sim$50 cm^{-3}) drops the autoconversion rate is $\sim 1.1 \times 10^{-3}$ s^{-1} (see Table 1). In order to study the two cases separately and to find out what changes in the cloud result from the contamination, we performed another 3-D LES run with the same initial sounding but with an optimization appropriate to a clean cloud. Figure 13 shows the computed LWC after four hours of simulation of the LES model. When compared with Figure 7 (representing the contaminated cloud) we not only find a significant decrease in the LWC but also the formation of an isolated cloud

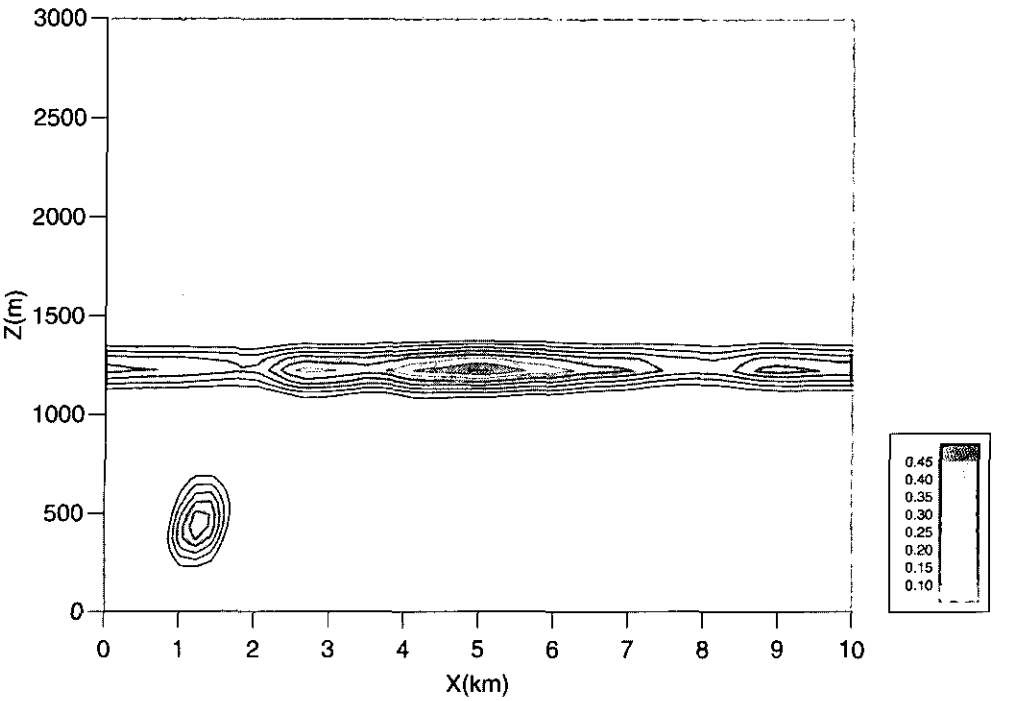

Figure 13. Liquid-water content (g m^{-3}) after four hours corresponding to a 'clean' optimization for the ACE-2 cloud after four hours of simulation of the LES model. See text for explanation.

patch in the subcloud layer. This results from the formation of drizzle which occurs more readily with the reduced droplet concentration.

From Eqs. (1)–(3) we find that τ is directly proportional to the cloud geometric thickness, and also depends on the LWC ($\tau \sim q_\ell^{2/3}$) and the droplet number concentration ($\tau \sim N^{1/3}$). We have seen that the effect of pollutants causes an increase in N with a corresponding decrease in the droplet sizes. This inhibits drizzle and results in a geometrically thicker cloud with higher LWC, and all these combine together to yield higher optical depths.

An observed aerosol spectrum was available and this was used to run the 1-D microphysical model. Measurements of the aerosol size distribution were obtained with a Passive Cavity Aerosol Spectrometer Probe for a size range between 0.05 and 1.5 μm radius; for larger particles, between 1.5 and 23.5 μm radius, the measurements were made using the FSSP. From an analysis of the chemical composition of the aerosol it was ascertained that in the small-size category with aerosol radius smaller that 0.75 μm the aerosol composition was dominated by $(NH_4)_2SO_4$, and for the larger ones with radii greater than 0.75 μm the aerosol particles were mainly sea salt (NaCl) (A. Dore 1999, personal communication). The input aerosol distribution for the microphysical model was constrained by the above information. The computed number concentrations are between 80 and 115 cm^{-3} with a size range of 6–10 μm radius and the largest drops close to the cloud top. These values, and in particular the predicted drop-size distribution away from the cloud top agree extremely well with the measured drop-size distribution with 90–150 cm^{-3} for droplet radii between 6 and 8 μm. Runs of the model in which

the concentration of HNO_3 was 5 p.p.t.v. (the observed value (Dore *et al.* 1998)) suggest that this did not significantly affect the droplet concentration or size distribution.

In this context it would be pertinent to recall the study by Fitzgerald (1974) of the effect of aerosol composition on the drop-size distribution. This showed that the drop-size distribution, resulting from condensation upon a population of mixed nuclei composed of both soluble and insoluble components, is generally not much broader than that produced by condensation upon a population of pure NaCl nuclei. It was also shown that, although the dispersion of cloud droplet sizes is quite insensitive to the variations in the percentages of the different nucleus types, the cloud-droplet number density decreases as the percentage of the more insoluble nuclei increases. In view of these results we performed a microphysical model run comprising a pure $(NH_4)_2SO_4$ CCN spectrum and we observed that there was indeed a small increase in the droplet number concentrations associated with only a small shift of the spectra by 0.5 μm towards larger radii. Our original run based on observed values has a CCN spectrum composed of NaCl in addition to $(NH_4)_2SO_4$. Since NaCl is less soluble than $(NH_4)_2SO_4$, the number density is slightly smaller, with an associated shift towards the smaller radii for this case in comparison with the run with only $(NH_4)_2SO_4$.

From an analysis of air parcel trajectories for the ACE-2 cloud, it is found that the air parcels only just skimmed the coast of France and Spain accounting for the cloud being only weakly polluted; as a result one could class this cloud to be more akin to a 'marine-type' cloud. The EUCREX cloud, however, has microphysical attributes that are more 'continental'. Also, for the ACE-2 simulation, not only were the acid levels 1/2000th of those of the EUCREX runs, the updraught velocities were almost double. Consequently the role of the HNO_3 in the activation process was much curtailed, since the water saturation itself was high enough to activate a substantial fraction of the aerosol particles.

7. Conclusions

In this study we have attempted to consolidate the main experimental observations available from the two recent European stratocumulus-related field projects i.e. the EUCREX and the ACE-2, and we have also sought to elucidate the various mechanistic details governing the dynamical, microphysical, and radiative properties of the two clouds through numerical modelling. A simple and cost-effective optimization of the classic Kessler scheme was applied to our case-studies. The overall cloud structure was well resolved by the optimized scheme and the model showed very realistic cloud-base and cloud-top undulations. The cloud thickness, the LWC and the droplet effective radii predicted by the models are in good agreement with the observations. The predicted optical depths for both clouds yield values comparable to the observations. Our calculations include the effect of a second condensible vapour (HNO_3) very likely to be present in polluted atmospheres. Pollutant gases can result in some alteration of the composition of the CCN spectrum leading to changes in the droplet spectrum. However, the major effect of pollutant vapours is to cause a decrease in the effective vapour pressure of water over the growing solution droplets and, as a consequence of this, a higher fraction of the particles can serve as CCN. Our calculations show that the overall effect of including HNO_3 is to decrease the mean size of the droplets, as the available vapour is now distributed between a larger number of activated particles. This inhibits drizzle and results in a geometrically thicker cloud with higher LWC, and all these combine together to yield higher optical depths.

The model results indicate that HNO_3 pollution is far more likely for the EUCREX cloud, resulting in significant alterations of the microphysical properties. For the ACE-2 cloud, even on a typical polluted day when the ambient HNO_3 level is unlikely to exceed 5 p.p.t.v., the model is insensitive to changes in HNO_3 concentrations less than 5 p.p.t.v.

ACKNOWLEDGEMENTS

We are grateful to Hanna Pawlowska and Jean-Louis Brenguier for many useful discussions particularly with regard to the EUCREX measurements, to the Met. Research Flight staff and air crew involved with the C-130 ACE-2 campaign and to Lothar Schüller for providing the OVID optical depths. S. Ghosh acknowledges the Natural Environment Research Council for financial assistance.

REFERENCES

Albrecht, B. A. 1989 Aerosols, cloud microphysics and fractional cloudiness. *Science*, **245,** 1227–1230

Albrecht, B. A., Randall, D. A. and Nicholls, S. 1988 Observations of marine stratocumulus during FIRE. *Bull. Am. Meteorol. Soc.*, **69,** 618–626

Albrecht, B. A., Bretherton, C. S., Johnson, D., Shubert, W. H. and Frisch, A. S. 1995 The Atlantic stratocumulus transition experiment—ASTEX. *Bull. Am. Meteorol. Soc.*, **76,** 889–904

Berry, E. X. 1968 'Modification of the warm rain process'. Pp. 81–88 in Proceedings of the first international conference on weather modification, 28 April–1 May 1968, Albany, New York. American Meteorological Society, State University of New York, Albany

Brenguier, J. L., Pawlowska, H., Schüller, L., Preusker, R., Fischer, J. and Fouquart, Y. 2000 Radiative properties of boundary layer clouds: droplet effective radius versus number concentration. *J. Atmos. Sci.*, **57,** 803–821

Cahalan, R. F., Ridgway, W., Wiscombe, W. J., Bell, T. L. and Snider, J. B. 1994 The albedo of fractal stratocumulus clouds. *J. Atmos. Sci.*, **51,** 2434–2455

Clark, T. L. 1976 Use of log–normal distributions for numerical calculation of condensation and collection. *J. Atmos. Sci.*, **30,** 857–878

Davis, A., Marshak, A., Wiscombe, W. and Cahalan, R. 1996 Scale invariance of liquid water distributions in marine stratocumulus. Part I: Spectral properties and stationarity issues. *J. Atmos. Sci.*, **53,** 1538–1558

Derbyshire, S. H., Brown, A. R. and Lock, A. P. 1994 The Meteorological Office large eddy simulation model. Met O (APR) Turbulence and Diffusion Note, No. 213 (available from the National Meteorological Library)

Deschamps, P. Y., Breon, F. M., Leroy, M., Podaire, A., Bricaud, A., Buriez, J. C. and Seze, G. 1994 The POLDER mission: instrument characteristics and scientific objectives. *IEEE Trans. Geosci. Remote Sensing*, **32,** 598–615

Descloitres, J., Pawlowska, H., Pelon, J., Brenguier, J. L., Parol, F., Buriez, J. G. and Flamant, P. 1996 'Experimental retrieval of cloud optical thickness during EUCREX: Comparison of three approaches'. Pp. *394–397* in Proceedings of the 12th international conference on clouds and precipitation, 19–23 August 1996, Zurich, Switzerland, Vol. I. International Commission on Clouds and Precipitation

Dore, A. J., Johnson, D. W., *Choularton, T. W.*, Osborne, S. R. and Bower, K. N. 1998 'Cloud processing of aerosol particles due to aqueous phase *chemical reactions during the ACE-2 Lagrangian experiment*'. Pp. 159–160 in Proceedings of AMS Conference on cloud physics, 17–21 August, Everett, Washington. American Meteorological Society

Feingold, G., Walko, R. L., Stevens, B. and Cotton, W. R. 1998 Simulations of marine stratocumulus using a new microphysical parameterisation scheme. *Atmos. Res.*, **47–48,** 505–528

Fitzgerald, J. W. 1974 Effect of aerosol composition on cloud droplet size distribution: A numerical study. *J. Atmos. Sci.*, **31,** 1358–1367

Ghosh, S. and Jonas, P. R. 1998 On the application of the classic Kessler and Berry schemes in Large Eddy Simulation Models *with a particular* emphasis on cloud autoconversion, the onset time of precipitation, and droplet evaporation. *Annales Geophysicae*, **10,** 628–637

Kessler, E. 1969 On the distribution and continuity of water substance in atmospheric circulations. *Meteorol. Monogr.*, **32,** 1–84

Kulmala, M., Laarksonen, A., Korhonen, P., Vesala, T., Ahonen, T. and Barrett, J. C. 1993 The effect of atmospheric nitric acid vapor on cloud condensation nucleus activation. *J. Geophys. Res.*, **98,** 22949–22958

Leaitch, W. R., Isaac, G. A., Strapp, J. W., Banic, C. M. and Wiebe, H. A. 1992 The relationship between cloud droplet number concentration and anthropogenic pollution: Observations and climatic implications. *J. Geophys. Res.*, **97,** 2463–2474

Mackay, G. I., Schiff, H. I., Wiebr, A. and Anlauf, K. 1988 Measurements of NO_2, H_2CO and HNO_3 by tunable laser absorption spectroscopy during the 1985 Clarement intercomparison study. *Atmos. Environ.*, **22,** 1555–1564

Marshak, A., Davis, A., Wiscombe, W. and Cahalan, R. 1997 Scale invariance of liquid water distributions in marine stratocumulus. Part II: Multifractal properties and intermittency issues. *J. Atmos. Sci.*, **54,** 1423–1444

Martin, G. M., Johnson, D. W. and Spice, A. 1994 The measurement and parameterization of effective radius of droplets in warm stratocumulus clouds. *J. Atmos. Sci.*, **51,** 1822–1842

Mason. P. J. 1989 Large eddy simulation of the convective boundary layer. *J. Atmos. Sci.*, **46,** 1492–1516

Mason, B. J. and Jonas P. R. 1974 The evolution of droplet spectra and large droplets by condensation in cumulus clouds. *Q. J. R. Meteorol. Soc.*, **100,** 23–28

Moeng, C. H. 1986 Large-eddy simulation of a stratus topped boundary layer: I. Structure and budget. *J. Atmos. Sci.*, **43,** 2886–2900

Nicholls, S. 1987 A model of drizzle growth in warm stratocumulus clouds. *Q. J. R. Meteorol. Soc.*, **113,** 1141–1170

Pasquier, J. 1996 'Large-eddy simulation of warm cumulus clouds'. PhD Thesis, UMIST, UK

Pawlowska, H. and Brenguier, J. L. 1996 'A study of the microphysical structure of stratocumulus clouds'. Pp. 23–26 in Proceedings of the 12th international conference on clouds and precipitation, 19–23 August 1996, Zurich, Switzerland, Vol. I. International Commission on Clouds and Precipitation

1998 'Microphysical properties of marine stratocumulus clouds', Pp. 310–313 in proceedings of AMS conference on cloud physics, 17–21 August, Everett, Washington. American Meteorological Society

Pawlowska, H., Brenguier, J. L. and Burnet, F. 2000 Microphysical properties of stratocumulus clouds. *Atmos. Res.* (in press)

Penner, J. E., Atherton, C. S., Dignon, J., Ghan, S. J. and Walton, J. J. 1991 Tropospheric nitrogen: A three-dimensional study of sources, distributions and deposition. *J. Geophys. Res.*, **96,** 959–990

Raes, F., Bates, T., Verver, G., McGovern, F. and Van Liederkerke, M. 2000 The second aerosol characterisation experiment (ACE-2): Introduction, meteorological overview and main results. *Tellus*, **52B,** 111–126

Raga, G. B. and Jonas, P. R. 1993 Microphysical and radiative properties of small cumulus clouds over the sea. *Q. J. R. Meteorol. Soc.*, **119,** 1399–1407

Seinfeld, J. H. 1986 *Atmospheric chemistry and physics of air pollution.* John Wiley, New York

Schüller, L., Fischer, J., Armbruster, W. and Bartsch, B. 1997 Calibration of high resolution remote sensing instruments in the visible and near infrared. *Adv. Space Res.*, **19,** 1325–1334

Schüller, L., Armbruster, W. and Fischer, J. 2000 Retrieval of cloud optical and microphysical properties from multi-spectral radiances. *Atmos. Res.* (in press)

Slingo, A. 1990 Sensitivity of the earth's radiation budget to changes in low clouds. *Nature*, **343,** 49–51

Slingo, A. and Wilderspin, R. 1986 Development of a revised long-wave radiation scheme for an atmospheric general-circulation model. *Q. J. R. Meteorol. Soc.*, **112,** 371–386

Twomey, S. 1977 The influence of pollution on the shortwave albedo of clouds. *J. Atmos. Sci.*, **34,** 1149–1152